OXFORD Toxicology Research

Toxicology Research, 2021, **10**, 264–271

doi: 10.1093/toxres/tfaa112
Advance Access Publication Date: 9 March 2021
Paper

PAPER

Cytotoxicity and DNA damage evaluation of TiO_2 and ZnO nanoparticles. Uptake in lung cells in culture

K. Freire,[1] F. Ordóñez Ramos,[2] D.B. Soria,[1] E. Pabón Gelves[2] and A.L. Di Virgilio[1,3,*]

[1]CEQUINOR, (CONICET-UNLP), Bv. 120 N 1465, La Plata, Argentina, [2]Escuela de Química, Facultad de Ciencias, Universidad Nacional de Colombia, sede Medellín. Cra 65 #59A -110, Medellín, Colombia, and [3]Facultad de Ciencias Exactas, Universidad Nacional de La Plata, 47 y 115 (1900), La Plata, Argentina

*Correspondence address. CEQUINOR, Facultad de Ciencias Exactas, UNLP, Bv. 120 N 1465 (1900) La Plata, Argentina. E-mail: aldivirgilio@biol.unlp.edu.ar

Abstract

The cytotoxicity and DNA damage of titanium dioxide and zinc oxide nanoparticles (TiO_2 and ZnO NPs) have been studied in a human lung carcinoma cell line (A549) after 24 h exposure. TiO_2 and ZnO NPs had mean diameters of 12.9 ± 2.8 and 24.1 ± 8.0 nm, respectively. ZnO NPs reduced cell viability from 250 μg/mL, increasing reactive oxygen species (ROS) and decreased GSH/GSSG ratio. The comet assay detected DNA damage from 50 μg/mL. TiO_2 NPs induced cytotoxicity and DNA damage from 50 to 100 μg/mL, respectively, along with a decrease of the GSH/GSSG ratio. Both particles were found inside the cells, within membrane-bound vesicles. The internalization mechanism is promoted partially by caveolae-mediated endocytosis and, in the case of TiO_2 NPs, also by macropinocytosis.

Key words: TiO_2 and ZnO nanoparticles, cytotoxicity, DNA damage, lung cells in culture, nanoparticles uptake

Introduction

Nanoparticles (NPs) are any particulate material with at least one dimension in the nanometer scale (1–100 nm) whose physical and chemical properties significantly differ from their bulk material, such as the high reactivity and physicochemical dynamics [1]. Engineered NPs with a structure and specific physicochemical composition are associated with cosmetics, food packaging, drug delivery systems, therapeutic products, biosensors, wound dressings, detergents, and antimicrobial coatings [2]. Moreover, nanomedicine involves the use of nanoparticles for therapeutic and diagnostic purposes [3].

Industrial exposure to inhaled NPs represents a substantial concern for worker's well-being [4]. The most significant exposure occurs when NPs are suspended in the air during production stages through handling, aerosolization, weighting, sonication, and mixing [5]. Inhaled nanomaterials with higher densities are more capable of reaching the lung's deeper regions placing in the respiratory alveolar region [6]. The alveolar epithelium consists of two different cell types; type I cells (which constitute more than 90% of the alveolar surface) are essential in transepithelial transport and cell signaling [7], and type II cells (covering 10% of the surface) synthesize and release pulmonary surfactant, a fluid rich in phospholipids that reduces surface tension in the liquid–air interface [8]. Because the lung's alveolar region provides a pathway to the rest of the body, the transport of NPs to this region is of most serious concern [6]. A study reported that inhaled nanoparticles are taken up and translocated across the pulmonary epithelium, a process controlled by alveolar type I epithelial cells [9].

The particles are incorporated by pathways that depend on size, shape, and surface chemistry [10]. Monocytes, macrophages, and neutrophils take up micrometer-sized particles by the

Received: 22 June 2020; **Revised:** 8 December 2020; **Accepted:** 21 December 2020

process of phagocytosis. On the other hand, NPs internalize by macropinocytosis or endocytosis mediated by caveolae and clathrin [11]. In the mechanism of macropinocytosis, vesicles form in the cell membrane (lamellipodia) upon growth factors stimulation by internalizing fluids and particles simultaneously. Moreover, many cell types—apart from the macrophage—utilize the clathrin-mediated and caveolin-mediated endocytosis pathway to internalize nanometer-scale materials, including viruses and particles [12, 13].

In this context, it is crucial to evaluate the safety of nanoparticles. It is presently not possible to make general statements and recommendations about the safety of nanoparticles because of the wide range of materials and particle sizes involved [3]. Given these uncertainties, our primary goal was to evaluate the cytotoxic effect and the DNA damage of two metal oxide nanoparticles on lung cells in culture, since inhalation is considered an important route of exposure to NPs, especially in occupational settings. We hypothesized that toxicological effects would depend on the chemical nature and size of NPs. Our studies also investigated the role of oxidative stress and the mechanism of NP internalization into cells.

Materials and methods

Materials

Tissue culture materials were purchased from Corning (Princeton, NJ, USA) and APBiotech (Buenos Aires, Argentina). Dulbecco's Modified Eagle Medium (DMEM) and TrypLE™ from Gibco (Gaithersburg, MD, USA), and fetal bovine serum (FBS) from Internegocios SA (Buenos Aires, Argentina). Dihydroethidium (DHE) was obtained from Molecular Probes® (Eugene, OR, USA). Reduced glutathione (GSH), o-phthalaldehyde (OPT), n-ethylmaleimide (NEM), and agaroses were acquired from Sigma Aldrich (St. Louis, MO, USA). A549 (CCL-185) cell line was purchased from ATCC®.

Synthesis and physicochemical characterization of TiO_2 and ZnO NPs

TiO_2 NPs were prepared by the sol–gel method reported by [14], using titanium isopropoxide as precursor and isopropanol as the solvent. HNO_3 was used as a catalyst, for which we used 250 mL of deionized water, and adjusted the pH to 2 with 3 M nitric acid. The precursor solution was added dropwise to the catalyst solution. The sample was dried at 100°C for 5 h and calcined at 400°C for 2 h.

ZnO NPs were synthesized by the controlled precipitation method reported by [15], using zinc acetate dihydrate in isopropanol as a precursor at 80°C under a reflux system using a molar ratio of 0.0085 ($Ac_2Zn.2H_2O$/iPrOH). Then, a methanolic KOH solution was added dropwise to the precursor solution. The solid obtained was dried at 60°C for 12 h and finally calcined at 400°C for 2 h.

The oxides obtained were characterized by X-ray diffractometry (XRD) and transmission electron microscopy (TEM). A X'Pert PRO MPD Panalytical Diffractometer was used for the analysis of crystalline phases, with registration from 0 to 100° in 2θ, scanning step of 0.05°, with Cu Kα anode ($\lambda = 1.54056$ Å). The morphology and size of the particles were determined by TEM (Tecnai G2 F20 microscope). For this purpose, we placed a powder sample—previously dispersed in ethanol—on a grid with carbon film.

Fresh stock suspensions of TiO_2 and ZnO NPs were prepared in phosphate-buffered saline (PBS) at 10 mg/mL, sonicated for 60 min, and stored at 4°C the dark. The stock suspension was diluted with Dulbecco's Modified Eagle Medium (DMEM) to obtain test dispersions at experiments' concentrations.

Cell culture

A549 human lung carcinoma epithelial cells and MRC-5 normal diploid human fibroblast were cultured in DMEM supplemented with 10% FBS, 100 U/mL penicillin, and 100 µg/mL streptomycin at 37°C in a humidified atmosphere with 5% of CO_2. The cells were seeded in a T75 flask until 80–90% of confluence and subcultured using TrypLE™. The experiments were carried out in multiwell plates, where cells were allowed to attach, and washed with DMEM before each treatment.

Cell viability assay

Monolayer cell viability was determined using 3-(4,5-dimethylthiazol-2-yl)-2,5-diphenyltetrazolium bromide (MTT), which is reduced by mitochondria in viable cells to a purple formazan dye [16]. Briefly, 2.5×10^4 cells were seeded on 96-well plates and incubated at 37°C. After 24 h, cells were exposed to different suspensions of each NP for 24 h. Afterward, the monolayers were washed and incubated with 0.5 mg/mL of MTT in DMEM for 3 h. We recorded the formazan absorbance extracted with DMSO (100 µL/well) at a wavelength of 570 nm using a multiplate reader Multiskan FC (Thermo Scientific). The cell viability is shown graphically as a percent of the control value.

DNA damage evaluation

For the detection of DNA damage, the single cell gel electrophoresis assay (Comet assay) was employed based on [17] with minor modifications. Briefly, A549 cells were treated with different concentrations of the NPs. After 24 h, cells were suspended in 0.5% low melting point agarose and immediately poured onto microscope slides precoated with 0.5% normal melting point agarose. The slides were immersed in ice-cold lysis solution (2.5 M NaCl, 100 mM Na_2-EDTA, 10 mM Trizma–HCl, pH 10 and 1% Triton X-100, 10% DMSO at 4°C, pH 10) for 1 h to lyse the cells, to remove cellular proteins, and to allow DNA unfolding. Then, the slides were placed on a horizontal gel electrophoresis tank, and the DNA was allowed to unwind for 20 min in freshly prepared alkaline electrophoresis buffer (300 mM NaOH and 1 mM Na_2-EDTA, pH 12.7). Electrophoresis was carried out in the same buffer for 30 min at 25 V (≈0.8 V/cm across the gels and ≈ 300 mA) in an ice bath condition. Afterward, we neutralized the slides and stained with Syber Green. The analysis was performed in an Olympus BX50 fluorescence microscope. A total of 200 randomly captured cells were used to determine the tail moment per experimental point using Comet Score version 1.5 software. We harvested the cells just before a pulse of 20 min of 10 µg/mL bleomycin, employed as the positive control.

Oxidative stress determination

Reactive oxygen species (ROS) induction was investigated as a mechanism of cell death employing a fluorescent probe dihydroethidium (DHE). It detects O2•¯, H2O2, ONOO¯, HOCl) [18]. 1×10^5 A549 cells were seeded in 24 well plates and incubated for 24 h. The culture medium was replaced with different concentrations of the NPs for 24 h. The cellular monolayer was

washed with PBS and incubated with DHE (10 µM) at 37°C for 30 min. Cells were washed and lysed with Triton X-100 0.1% for 30 min. The cell extracts were then analyzed for the oxidized product (ethidium) by measuring fluorescence (excitation wavelength 518 nm; emission wavelength 605 nm), using a Shimadzu Spectrofluorophotometer RF-6000 equipped with a computer working with LabSolutions RF software. Results were corrected for protein content and measured with the Pierce™ BCA Protein Assay Kit.

Reduced (GSH) and oxidized (GSSG) glutathione levels were determined as described by [19]. Confluent A549 monolayer cultured in 24-well plates was treated with different TiO_2 or ZnO suspensions for 24 h. Then, the monolayer was washed with PBS, and the cells were lysed with 250 µL 0.1% Triton X-100 for 30 min at 4°C. For GSH determination, 100 µL of the cellular lysate was added to 1.8 mL of ice-cold phosphate buffer (Na_2HPO_4 0.1 M EDTA 0.005 M pH 8.0) and 100 µL o-phthaldialdehyde (0.1% in methanol). For the determination of GSSG, 100 µL of the cell lysate were mixed with 20 µL 0.04 M of N-ethylmaleimide for 20 min at 4°C, then 1.8 mL of NaOH 0.1 M were added. Fluorescence was registered using a fluorometer Shimadzu RF-6000, the samples were excited at 350 nm, and the emission signal was acquired at 420 nm. GSH/GSSG ratio was calculated as % of the basal for all the experimental conditions.

Uptake and subcellular localization by TEM

A549 cells were treated with 0.2-mM genistein or 1-mM amiloride to inhibit the caveolae-mediated endocytosis or macropinocytosis, respectively [20, 21]. After 30 min, 50 µg/mL TiO_2 or ZnO NPs were added for 3 h. Cells treated only with the NPs were used as control. Cells were fixed in 2% glutaraldehyde in 0.1-M sodium cacodylate buffer for 1 h at 4°C, followed by treatment with 2% OsO4 in sodium cacodylate. Then, cells were embedded in epoxy resin, Epon (Serva, Heidelberg, Germany). Ultrathin sections (60 nm) were obtained by ultramicrotome (Supernova Reichert-J). These sections were stained with an 8% uranyl acetate solution in 0.5% acetic acid and plumbic citrate. These sections were placed on 150 mesh grids and examined with a TEM microscope (JEOL Ltd., Tokyo, Japan). The images were captured with a digital camera (Erlangshen ES1000W, Model 785. Gatan Inc., Pleasanton, California, USA) from the Central Electron Microscopy Service (Facultad de Ciencias Veterinarias, UNLP). TEM analysis allowed determination of the agglomeration of the particles and their distribution within the cells.

Statistical analysis

Results are expressed as the mean of three independent experiments and plotted as the mean ± standard error of the mean (sem). The total number of repeats (n) is specified in the legends of the figures. The statistical analysis was carried out by ANOVA, followed by the Fisher' Least Significant Difference (LSD) procedure to discriminate among the means. The statistical analyses were performed using STATGRAPHICS Centurion XVI.I. The level of significance is established in Results and Figure Captions.

Results

Physicochemical characterization of the materials

XRD confirmed the crystallization of the TiO_2 NPs. The X-ray diffractogram of calcined materials (Fig. 1A) showed one prominent peak at $2\theta = 25.35°$ corresponding to the anatase phase.

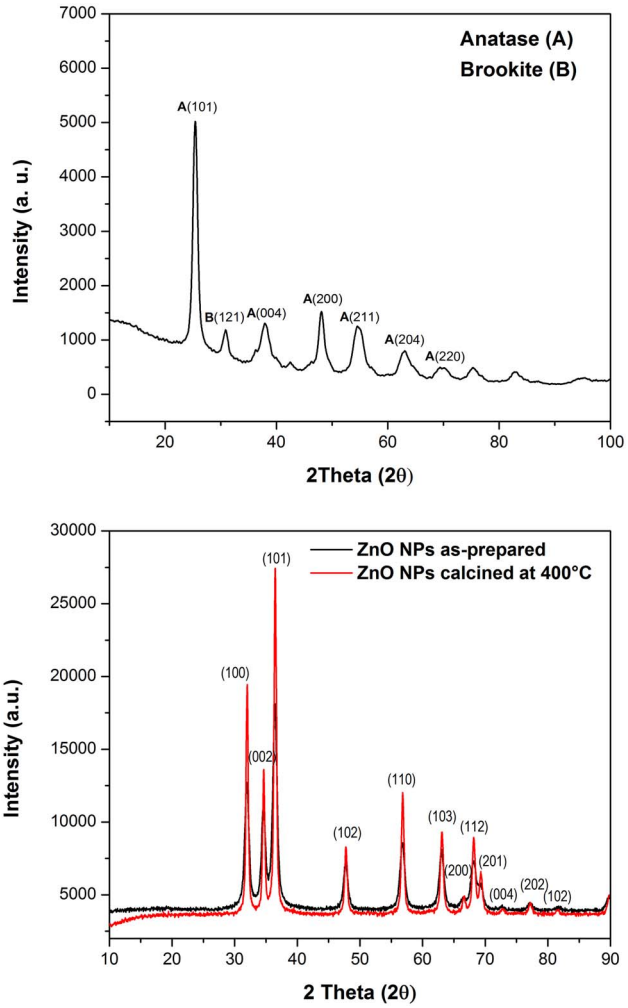

Figure 1: X-ray diffractogram of TiO_2 (**A**) and ZnO (**B**) NPs.

Other peaks of lower intensity at 2θ = a 25.3, 38.8, 48.1 (anatase phase), and a peak in $2\theta = 30.8$ correspond to the brookite phase. The thermal treatment is appropriate for transformation from amorphous to the crystalline phase and the formation of phases such as anatase and brookite. Figure 1B shows defined peaks indicating that ZnO NPs are highly crystalline, with a polycrystalline structure. The pattern after calcination exhibits sharper peaks, indicating an enhancement of crystallinity as previously observed [22, 23]. The XRD peaks for planes (100), (002), and (101) indicate the pure phase formation of the wurtzite structure of ZnO. The crystallographic plane (101) in 2θ (36.24) exhibits a maximum, being the most prominent, so the growth orientation for these materials in this plane is associated with this crystalline phase of hexagonal wurtzite.

According to TEM results, TiO_2 NPs are spheric and have nanometric sizes. Agglomerates of particles are visualized as well. Such groups are composed of primary particles, with sizes greater than 100 nm, due to the particles' high surface energy, which produces variable size agglomerates. An average value of particle size of 12.9 ± 2.8 nm was determined.

The study of morphology by TEM determined that the shape of ZnO NPs corresponds to irregular hexagons, and small agglomerates composed of primary particles with sizes from 20 to 50 nm are observed. The average value of particle size is 24.1 ± 8.0 nm.

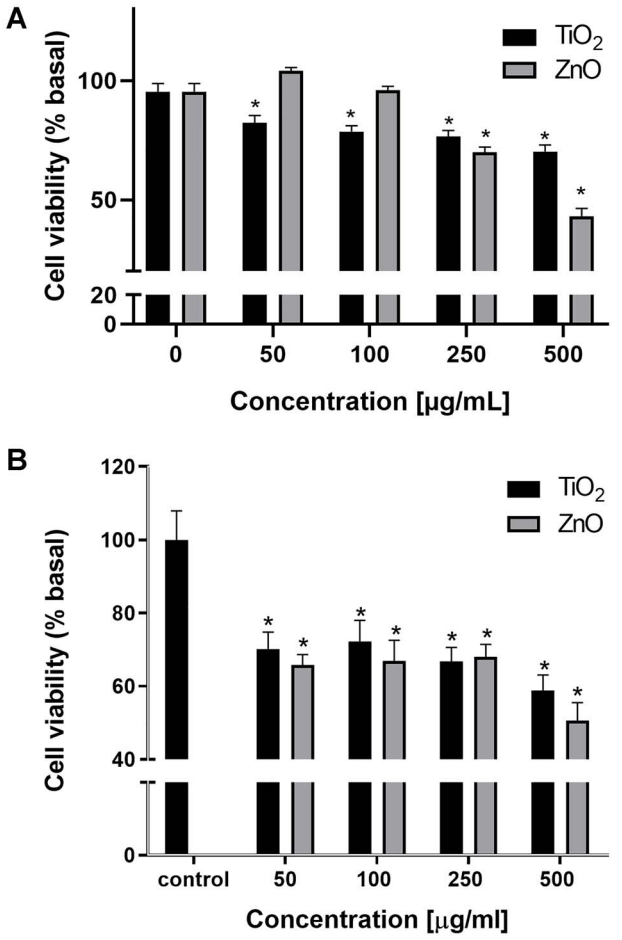

Figure 2: Effect on cell viability of TiO_2 and ZnO NPs in A549 cells (**A**) and MRC-5 cells (**B**). Asterisks represent statistically significant difference with solvent control (*$p < 0.05$).

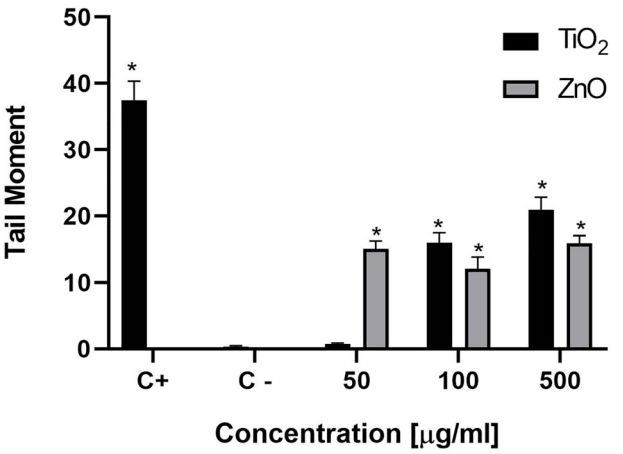

Figure 3: DNA damage studied by the Comet assay in A549 cells treated with TiO_2 or ZnO NPs during 24 h. Asterisks (*) represent a statistically significant difference with control cells ($p < 0.05$).

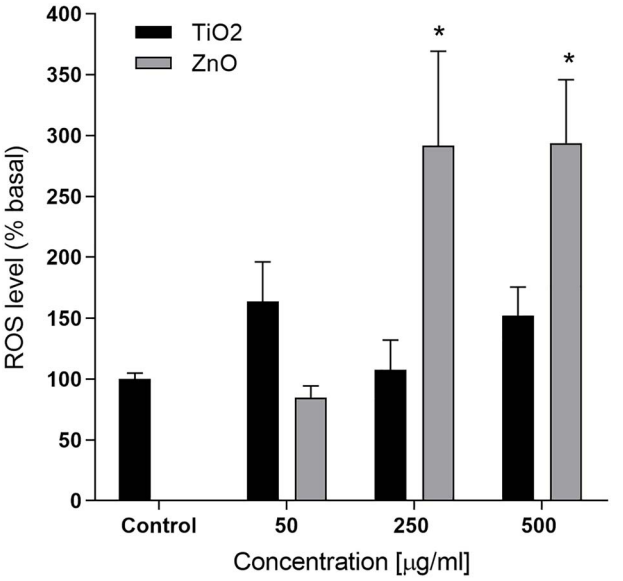

Figure 4: Effect of ROS induction by TiO_2 or ZnO NPs in A549 cells. Asterisks (*) represent statistically significant difference with solvent control $p < 0.05$).

Effect of TiO_2 and ZnO NPs on cell viability

The cytotoxicity of TiO_2 and ZnO NPs was assayed in 24-h exposed A549 and MRC-5 cells by measuring the ability to process MTT. Figure 2 shows the relationship between cell viability (as percentage absorbance of control value) and particle concentration. Alteration in cell energy metabolism can be monitored by measuring the loss of mitochondria's ability to reduce MTT to an insoluble violet product (formazan) and cell viability. Exposing A549 cells to dispersions of either TiO_2 or ZnO NPs at different concentrations (50–500 µg/mL) showed that only TiO_2 NPs induced a statistically significant decrease of around 20% in the ability of the cells to form the insoluble violet product in the whole range of concentrations tested (Fig. 2A, $P < 0.05$). However, ZnO NPs caused a statistically significant decrease only at the higher tested concentrations (250 and y 500 µg/mL), but the effect on cell viability exceeded 50% (Fig. 2A). On the other hand, Figure 2B shows that both particles exert cytotoxicity on MRC-5 cells, stressing the effect at the highest concentration tested.

DNA damage of TiO_2 and ZnO NPs on A549 cells

Figure 3 shows the Tail Moment as a function of the concentration. This parameter takes into account the length and fluorescence intensity of the tail of the comet. A statistically significant increase can be observed from 50 µg/mL ZnO and 100 µg/mL TiO_2 compared to the negative control, in which the cells were incubated only with culture medium ($P < 0.05$). However, the increase was less pronounced than that exerted by the positive control. Only TiO_2 NPs-treated cells showed a statistically significant dose–response effect ($P < 0.05$).

Effect of TiO_2 and ZnO NPs on oxidative stress

To better understand the possible mechanism involved in the cytotoxicity and DNA damage of TiO_2 and ZnO NPs in A549 cells, we evaluated the effect on oxidative stress by measuring ROS level by oxidation of the probe DHE. Only incubation of A549 cells with ZnO NPs caused a statistically significant increase in ROS level at the highest concentrations tested (250 and 500 µg/mL, Fig. 4) that tripled the basal level ($P < 0.05$).

To get a broader knowledge of the cellular redox status, we investigated the GSH/GSSG ratio. An increase in ROS levels may

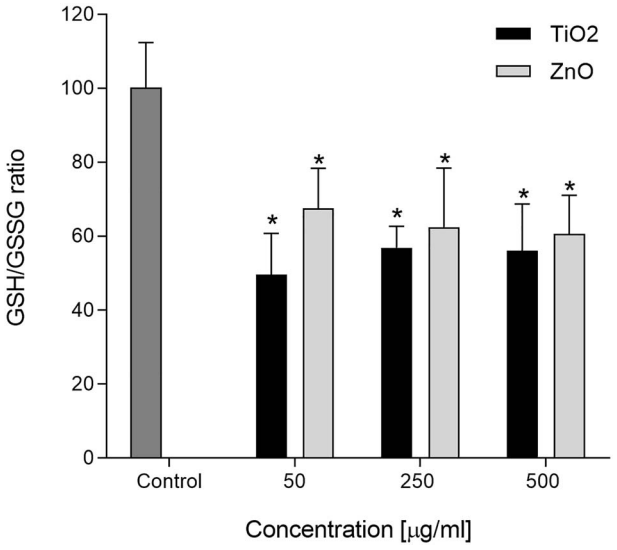

Figure 5: GSH/GSSG ratio in A549 cells after treatment with TiO_2 or ZnO NPs. Asterisks (*) represent statistically significant difference with solvent control ($p < 0.05$).

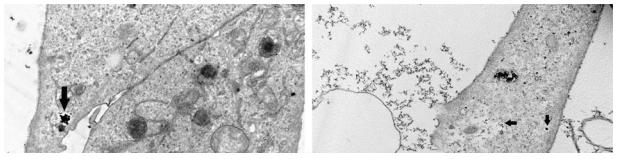

Figure 6: TEM images of A549 cells after treatment with 50 μg/ml ZnO (upper panel, left) or 50 μg/ml TiO_2 (upper panel, right) during 3 h. Black arrows indicate small agglomerations of NPs inside vesicles in the cells. Cells treated with genistein (0, 2 mM) for 30 min at 37 °C and exposed to TiO_2 NPs for 3 h (lower panel, left) Cells treated with amiloride (1 mM) for 30 min at 37 °C and exposed to TiO_2 NPs for 3 h (lower panel, right).

reduce GSH levels and accumulate GSSG inside the cells. Both TiO_2 and ZnO NPs induced a decrease in the GSH/GSSG ratio to approximately half the control value in A549 cells above 50 µg/mL ($P < 0.05$; Fig. 5).

Uptake and subcellular localization

Figure 6 shows A549 cells treated with 50 µg/mL ZnO (upper panel, left) and TiO_2 (upper panel) for 3 h in the absence of inhibitors. Their high electron density identifies NPs in contrast with cellular components. These micrographs revealed that both NPs-treated cells formed intracellular vesicles containing internalized material. It was observed that NPs formed agglomerates inside the vesicles in A549 cells. In addition, lamellipodia-like structures in the cell membrane were observed previous to the endocytosis (not shown).

A549 cells previously treated with inhibitors of specific internalization mechanisms are shown in Figure 6 (lower panels). Cells were treated with genistein (caveolae-mediated endocytosis inhibitor) and TiO_2 NPs for 3 h (lower panel, left) and amiloride (macropinocytosis inhibitor) and TiO_2 NPs for 3 h (lower panel, right). In these cases, NPs are found exclusively on the outside of the cells, mainly in a chain arrangement on the outer face of the cytoplasmic membrane, and no NPs were found inside the cells. The same result was obtained in the treatment with ZnO NPs and genistein (data not shown); with amiloride, no cells were observed in the ultrathin sections.

Discussion

The great demand in the manufacture of materials in nanometric scale for uses in diverse fields has led to the investigation of toxic effects when they come into contact with living organisms. In particular, metal oxide nanoparticles are widely used in textile manufacturing, in solar screens, in cosmetics, and as antimicrobial agents for their photocatalytic activity under UV light. As their applications continue to expand, concerns have been mounting about the environmental fate and potential health risk [24]. Because NPs can be suspended in the air in the local environment during their manufacture, epithelial cells in the lung including those lining alveolar spaces are at risk of contact with the inhaled particles [25, 26]. For this reason, the effects of the particles on human type II pneumocytes represented by the A549 cell line were examined.

This study clearly shows that both TiO_2 and ZnO NPs altered the cell viability of lung epithelial cells. Several studies show cytotoxic effects of TiO_2 NPs in cell cultures such as bronchial, alveolar, colonic, and gastric epithelial cells [27–29]. However, investigations on TiO_2 NPs in A549 cells with other methods such as the Neutral Red uptake assay showed no toxic effect below 100 µg/mL [30]. Such effects are dependent on the size, concentration, and structure of the NPs, showing more significant toxicity at smaller sizes. Also, *in vivo* studies suggest that particles' inhalation produces severe lung inflammation and emphysema in the lungs of mice [31]. Studies conducted with ZnO NPs showed that the toxic effect is based on oxidative stress induction, inflammation, and DNA damage in cellular and animal models [32–34] and due to the release of Zn^{+2} ions [35]. Alteration of cellular Zn homeostasis in *in vitro* systems has been related to mitochondrial dysfunction [36], which leads to increased production of ROS and, eventually, cell death. Moreover, current findings demonstrated that a combination of Gd-doped ZnO NPs with X-rays induced dose-dependent radiosensitivity at lower concentrations (10 and 20 µg/mL) [37].

In addition, we also studied DNA damage in the A549 cells exposed to NPs using the comet assay (single-cell gel electrophoresis), one of the most common tests for measuring genotoxicity in cell cultures and tissues [38]. This assay detects breaks in the DNA and labile alkaline sites.

In accordance with our findings, several reports on TiO_2 NPs show genotoxic effects in cells of the bronchial epithelium and alveolar epithelium, inducing the generation of micronuclei—which indicates the presence of DNA breakage or chromosome loss—and cell damage [39, 40]. Studies conducted with ZnO NPs also indicate genotoxicity produced by ROS production in several cell cultures, such as human colon carcinoma cells, lung fibroblasts, and bronchial epithelial cells showing particularly DNA damage induction and micronuclei [41–43].

Oxidative stress and inflammation are the most important mechanisms for which nanomaterials induce genotoxicity [44]. ROS production is directly related to genotoxicity since it can cause direct damage by breaking the chains [45] or cause oxidative damage to the DNA by the oxidation of bases such as 8-oxo-7, dihydro-2′-deoxyguanosine [46, 47]. Therefore, we have investigated the cellular mechanisms that may trigger DNA damage in A549 cells by determining the oxidative stress caused by ROS's overproduction, leading to a decrease of GSH/GSSG ratio.

Our findings showed that only ZnO NPs-treated cells produce a statistically significant ROS level increment by converting DHE

to ethidium at high concentrations. It is reported that DHE freely permeates cell membranes and is relatively specific for superoxide ion [18]. However, when the dihydrorhodamine (which is oxidized by hydrogen peroxide) was employed, no increase could be detected for both NPs (data not shown). The relationship between ROS levels and GSH/GSSG ratio in ZnO-treated cells is relatively straightforward and could explain the cytotoxicity and the DNA damage. On the other hand, the connection between ROS levels and GSH/GSSG ratio in TiO_2-treated cells is very intricate since no evident correlation could be established. These NPs maintained ROS levels at control values determined by the DHE method. Nevertheless, they caused a decrease in the GSH/GSSG ratio of nearly 50%. A mechanism involved in the particle's deleterious action on these thiol-containing molecules may be related to the effect of other free radicals that cannot be detected by this fluorescent probe. These species have some characteristics that make them difficult to detect, such as their short life and the great variety of antioxidants existing, capable of capturing them [48].

Our findings show that ZnO NPs caused a cytotoxic effect in parallel with ROS induction from 250 µg/mL and DNA damage from 50 µg/mL, while TiO_2 NPs showed a less pronounced harmful effect on cell viability or DNA. The detection of ROS increase was not statistically significant. The differential response between these two NPs has also been reported. TiO_2 NPs did not exhibit any cyto- or genotoxic potential below 20 µg/mL; however, the study indicated cyto- and genotoxicity resulting from ZnO NPs in mucosa cells [49]. Furthermore, the mechanistic pathways involved in NPs' toxic effects triggering are complicated. Mitochondrial dysfunction, endoplasmic reticulum stress, and lysosomal rupture are involved in the process. The increased generation of ROS, a currently recognized mechanism for causing cell damage, is positively correlated with the degree of apoptosis, autophagy, and inflammation and plays a role in several signal pathways [50]. TiO_2 NPs induced ROS generation and mitochondrial membrane potential breakdown in human monocytes at lower concentrations [51]. ZnO NPs triggered an excessive ROS production, which then activates the apoptosis pathway mediated by mitochondria in zebrafish embryos [52].

The internalization of the NPs was investigated by TEM. It is well known that nanoparticles' internalization pathways depend on their size, shape, and surface chemistry [10]. Our findings showed a rapid internalization of the NPs inside the A549 cells, after the exposure for 3 h, in agreement with previous reports on ultrafine particles of TiO_2 in alveolar epithelial cells [53, 54]. In genistein-treated cells, caveolae-mediated endocytosis is inhibited, demonstrating that this is one of the mechanisms involved in TiO_2 and ZnO NPs internalization. These observations agree with studies conducted in bronchial epithelial cells, in which NPs enter the cell through caveolae [55]. Macropinocytosis is another way in which NPs TiO_2 enter the cells since the internalization was inhibited when they were treated with amiloride. This pathway was also described in the internalization of NPs in glial cells [56]. On the other hand, it has been shown that TiO_2 NPs in large aggregates can internalize by phagocytosis in A549 cells and smaller clusters by clathrin-mediated endocytosis [57].

Conclusion

Nanoparticles of metal oxides TiO_2 and ZnO were found to internalize inside cultured lung epithelial cells, and this was associated with a reduction in cell viability. Our results showed that these NPs internalize in small groups by caveolae-mediated endocytosis and macropinocytosis. Only ZnO NPs produced an increase in ROS formation detected by the oxidation of DHE; however, depletion of thiol-reducing agents could be observed for both NPs. This effect could lead to DNA damage detected by the comet assay.

Conflict of interest statement

There are no conflicts to declare.

Funding

This work was supported by UNLP (PPID 2018/X032) and ANPCyT (PICT 2016-0508) from Argentina and Universidad Nacional de Colombia (Hermes 35904) from Colombia.

References

1. Oberdörster G, Maynard A, Donaldson K et al. Principles for characterizing the potential human health effects from exposure to nanomaterials: elements of a screening strategy. *Part. Fibre Toxicol.* 2005;**35**:1–35. doi: 10.1186/1743-8977-2-8.
2. Ray PC, Yu H, Fu PP. Toxicity and environmental risks of nanomaterials: challenges and future needs. *J. Environ. Sci. Heal. Part C Environ. Carcinog. Ecotoxicol. Rev.* 2009;**27**:37–41. doi: 10.1080/10590500802708267.
3. Wolfram J, Zhu M, Yang Y et al. Safety of nanoparticles in medicine. *Curr. Drug Targets.* 2015;**16**:1671–81. doi: 10.2174/1389450115666140804124808.
4. Graczyk H, Riediker M. Occupational exposure to inhaled nanoparticles: are young workers being left in the dust? *J. Occup. Health.* 2019;**61**:333–8. doi: 10.1002/1348-9585.12056.
5. Maynard AD, Kuempel ED. Airborne nanostructured particles and occupational health. *J. Nanoparticle Res.* 2005;**7**:587–614. doi: 10.1007/s11051-005-6770-9.
6. Arick DQ, Choi YH, Kim HC, Won Y-Y. Effects of nanoparticles on the mechanical functioning of the lung. *Adv. Colloid Interface Sci.* 2015;**225**:218–28. doi: 10.1016/j.cis.2015.10.002.
7. Williams MC. Alveolar type I cells: molecular phenotype and development. *Annu. Rev. Physiol.* 2003;**65**:669–95. doi: 10.1146/annurev.physiol.65.092101.142446.
8. Fisher AB, Dodia C, Ruckert P et al. Pathway to lamellar bodies for surfactant protein a. *Am. J. Physiol. Llung Cell. Mol. Physiol.* 2010;**299**:51–8. doi: 10.1152/ajplung.00066.2010.
9. Thorley AJ, Ruenraroengsak P, Potter TE, Tetley TD. Critical determinants of uptake and translocation of nanoparticles by the human pulmonary alveolar epithelium. *ACS Nano.* 2014;**8**:11778–89. doi: 10.1021/nn505399e.
10. Oh N, Park J-H. Endocytosis and exocytosis of nanoparticles in mammalian cells. *Int. J. Nanomedicine.* 2014;**9**:51–63.
11. Geiser M. Update on macrophage clearance of inhaled micro- and nanoparticles. *J. Aerosol Med. Pulm. Drug Deliv.* 2010;**23**:207–17.
12. Wang Z, Tiruppathi C, Minshall RD, Malik AB. Size and dynamics of Caveolae studied using nanoparticles in living endothelial. *ACS Nano.* 2009;**3**:4110–6.
13. Mercer J, Schelhaas M, Helenius A. Virus entry by endocytosis. *Annu. Rev. Biochem.* 2010;**79**:803–33. doi: 10.1146/annurev-biochem-060208-104626.
14. Zapata PA, Palza H, Delgado K, Rabagliati FM. Novel antimicrobial polyethylene composites prepared by metallocenic in situ polymerization with TiO2-based nanoparticles, *J. Polym. Sci. Part A Polym. Chem.* 2012;**50**:4055–62. doi: 10.1002/pola.26207.

15. Pi S, Mucur II, Tumay TAI et al. Triangular-shaped zinc oxide nanoparticles enhance the device performances of inverted OLEDs. *Nano-Structures and Nano-Objects*, *14* 2015;**1**:7. doi: 10.1016/j.nanoso.2015.01.001.
16. T. Mosmann, Rapid colorimetric assay for cellular growth and survival: application to proliferation and cytotoxicity assays., *J. Immunol. Methods.* **65** (1983) 55–63. http://www.ncbi.nlm.nih.gov/pubmed/6606682.
17. Singh NP, McCoy MT, Tice RR, Schneider EL. A simple technique for quantitation of low levels of DNA damage in individual cells. *Exp. Cell Res.* 1988;**175**:184–91. doi: 10.1016/0014-4827(88)90265-0.
18. Yazdani M. Concerns in the application of fluorescent probes DCDHF-DA, DHR 123 and DHE to measure reactive oxygen species in vitro. *Toxicol. Vitr.* 2015;**30**:578–82. doi: 10.1016/j.tiv.2015.08.010.
19. Hissin PJ, Hilf R. A fluorometric method for determination of oxidized and reduced glutathione in tissues. *Anal. Biochem.* 1976;**74**:214–26. doi: 10.1016/0003-2697(76)90326-2.
20. Koivusalo M, Welch C, Hayashi H et al. Amiloride inhibits macropinocytosis by lowering submembranous pH and preventing Rac1 and Cdc42 Signaling. *J. Cell Biol.* 2010;**188**:547–63. doi: 10.1083/jcb.200908086.
21. Nabi IR, Le PU. Caveolae/raft-dependent endocytosis. *J. Cell Biol.* 2002;**7**:673–7. doi: 10.1083/jcb.200302028.
22. Zak AK, Abrishami ME, Majid WHA et al. Effects of annealing temperature on some structural and optical properties of ZnO nanoparticles prepared by a modified sol – gel combustion method. *Ceram. Int.* 2011;**37**:393–8. doi: 10.1016/j.ceramint.2010.08.017.
23. Wang H, Xie C. Effect of annealing temperature on the microstructures and photocatalytic property of colloidal ZnO nanoparticles. *J. Phys. Chem. Solids.* 2008;**69**:2440–4. doi: 10.1016/j.jpcs.2008.04.036.
24. Joo SH, Zhao D. Environmental dynamics of metal oxide nanoparticles in heterogeneous systems: a review. *J. Hazard. Mater.* 2017;**322**:29–47. doi: 10.1016/j.jhazmat.2016.02.068.
25. Dwivedi S, Saquib Q, Ahmad B et al. Toxicogenomics: a new paradigm for Nanotoxicity evaluation. *Adv. Exp. Med. Biol.* 2018;**1048**:143–61.
26. Detampel P, Id AG, Tehranian S et al. In vivo clearance of nanoparticles by transcytosis across alveolar epithelial cells. *PLoS One.* 2019;**14**:1–13. doi: 10.1371/journal.pone.0223339.
27. Guadagnini R, Moreau K, Hussain S et al. Toxicity evaluation of engineered nanoparticles for medical applications using pulmonary epithelial cells. *Nanotoxicology.* 2013;**5390**:1–8. doi: 10.3109/17435390.2013.855830.
28. Emadi A, Moshfegh S. Induction of apoptosis and inhibition of invasion in gastric cancer cells by titanium dioxide nanoparticles 1, Oman. *Med. J.* 2018;**33**:111–7. doi: 10.5001/omj.2018.22.
29. Gandamalla D, Lingabathula H, Yellu N. Nano titanium exposure induces dose- and size- dependent cytotoxicity on human epithelial lung and colon cells. *Drug Chem. Toxicol.* 2019;**42**:24–34. doi: 10.1080/01480545.2018.1452930.
30. Ivask A, Titma T, Visnapuu M et al. Toxicity of 11 metal oxide nanoparticles to three mammalian cell types in V. *itro, Curr. Top. Med. Chem.* 2015;**15**:1914–29. doi: 10.2174/1568026615666150506150109.
31. Chen H, Su S, Chien C et al. Titanium dioxide nanoparticles induce emphysema-like lung injury in mice. *FASEB J.* 2006;**20**:2393–5. doi: 10.1096/fj.06-6485fje.
32. Remzova M, Zouzelka R, Brzicova T et al. Toxicity of TiO_2, ZnO, and SiO_2 nanoparticles in human lung cells: safe-by-design development of construction materials. *Nanomaterials.* 2019;**9**:968–82.
33. Chen J, Ho C, Chang H et al. Particulate nature of inhaled zinc oxide nanoparticles determines systemic effects and mechanisms of pulmonary inflammation in mice. *Nanotoxicology.* 2014;**5390**:1–11. doi: 10.3109/17435390.2014.886740.
34. Saptarshi SR, Duschl A, Lopata AL. Biological reactivity of zinc oxide nanoparticles with mammalian test systems: an overview. *Nanomedicine.* 2015;**10**:2075–92.
35. George S, Pokhrel ŒS, Xia ŒT et al. Use of a rapid cytotoxicity screening approach to engineer a safer zinc oxide nanoparticle through iron doping. *ACS Nano.* 2010;**4**:15–29.
36. Kao Y, Chen Y, Cheng T et al. Zinc oxide nanoparticles interfere with zinc ion homeostasis to cause cytotoxicity. *Toxicol. Sci.* 2012;**125**:462–72. doi: 10.1093/toxsci/kfr319.
37. Zangeneh M, Nedaei HA, Mozdarani H et al. Enhanced cytotoxic and genotoxic effects of gadolinium-doped ZnO nanoparticles on irradiated lung cancer cells at megavoltage radiation energies. *Mater. Sci. Eng. C.* 2019;**103**:109739. doi: 10.1016/j.msec.2019.109739.
38. Doak SH, Dusinska M. NanoGenotoxicology: present and the future. *Mutagenesis.* 2017;**32**:1–4. doi: 10.1093/mutage/gew066.
39. Kansara K, Patel P, Shah D et al. TiO_2 nanoparticles induce DNA double strand breaks. *Environ. Mol. Mutagen.* 2014;**56**:204–17. doi: 10.1002/em.
40. Ghosh M, Öner D, Duca R et al. Mutation research/genome instability and disease Cyto-genotoxic and DNA methylation changes induced by different crystal phases of TiO2-np in bronchial epithelial (16-HBE) cells. *Mutat. Res. - Fundam. Mol. Mech. Mutagen* 2017;**796**:1–12. doi: 10.1016/j.mrfmmm.2017.01.003.
41. Ng CT, Yong LQ, Hande MP et al. Zinc oxide nanoparticles exhibit cytotoxicity and genotoxicity through oxidative stress responses in human lung fibroblasts and Drosophila melanogaster. *Int. J. Nanomedicine.* 2017;**12**:1621–37.
42. Roszak J, Catalan J, Jarventaus H et al. Effect of particle size and dispersion status on cytotoxicity and genotoxicity of zinc oxide in human bronchial epithelial cells. *Mutat. Res. - Fundam. Mol. Mech. Mutagen.* 2016;**805**:7–18. doi: 10.1016/j.mrgentox.2016.05.008.
43. Condello M, De Berardis B, Grazia M et al. Toxicology in vitro ZnO nanoparticle tracking from uptake to genotoxic damage in human colon carcinoma cells. *Toxicol. Vitr.* 2016;**35**:169–79. doi: 10.1016/j.tiv.2016.06.005.
44. Møller P, Danielsen PH, Karottki DG et al. Mutation research/reviews in mutation research oxidative stress and inflammation generated DNA damage by exposure to air pollution particles, Mutat. Res. *Mutat. Res.* 2014;**762**:133–66. doi: 10.1016/j.mrrev.2014.09.001.
45. Magdolenova Z, Collins AR, Kumar A et al. Mechanisms of genotoxicity. Review of recent in vitro and in vivo studies with engineered nanoparticles mechanisms of genotoxicity. A review of in vitro and in vivo studies with engineered nanoparticles. *Nanotoxicology* 2013;**8**:233–78. doi: 10.3109/17435390.2013.773464.
46. Shukla RK, Sharma V, Pandey AK et al. Toxicology in vitro ROS-mediated genotoxicity induced by titanium dioxide nanoparticles in human epidermal cells. *Toxicol. Vitr.* 2011;**25**:231–41. doi: 10.1016/j.tiv.2010.11.008.

47. Jugan M, Barillet S, Simon-deckers A et al. Titanium dioxide nanoparticles exhibit genotoxicity and impair DNA repair activity in A549 cells. *Nanotoxicology*. 2012;**6**:501–13. doi: 10.3109/17435390.2011.587903.
48. Gomes A, Fernandes E, Lima LFC. Fluorescence probes used for detection of reactive oxygen species. *J. Biochem. Biophys. Methods*. 2005;**65**:45–80. doi: 10.1016/j.jbbm.2005.10.003.
49. Hackenberg S, Scherzed A, Zapp A et al. Genotoxic effects of zinc oxide nanoparticles in nasal mucosa cells are antagonized by titanium dioxide nanoparticles. *Mutat. Res. - Genet. Toxicol. Environ. Mutagen*. 2017;**816–817**:32–7. doi: 10.1016/j.mrgentox.2017.02.005.
50. Liu N, Tang M. Toxic effects and involved molecular pathways of nanoparticles on cells and subcellular organelles. *J. Appl. Toxicol*. 2020;**40**:16–36. doi: 10.1002/jat.3817.
51. Ghanbary F, Seydi E, Naserzadeh P, Salimi A. Toxicity of nanotitanium dioxide (TiO_2-NP) on human monocytes and their mitochondria. *Environ. Sci. Pollut. Res*. 2018;**25**:6739–50. doi: 10.1007/s11356-017-0974-2.
52. Zhao X, Ren X, Zhu R et al. Zinc oxide nanoparticles induce oxidative DNA damage and ROS-triggered mitochondria-mediated apoptosis in zebrafish embryos. *Aquat. Toxicol*. 2016;**180**:56–70. doi: 10.1016/j.aquatox.2016.09.013.
53. Stearns RC, Paulauskis JD, Godleski JJ. Endocytosis of ultrafine particles by A549 cells. *Am. J. Respir. Cell Mol. Biol*. 2001;**24**:108–15.
54. Andersson PO, Lejon C, Ekstrand-hammarström B et al. Polymorph- and size-dependent uptake and toxicity of TiO_2 nanoparticles in living lung epithelial cells. *Small*. 2011;**7**:514–23. doi: 10.1002/smll.201001832.
55. Xia T, Kovochich M, Liong M et al. Comparison of the mechanism of toxicity of zinc oxide and cerium oxide nanoparticles based on dissolution and oxidative stress properties. *ACS Nano*. 2008;**2**:2121–34.
56. Huerta-Garcia E, Marquez-Ramirez SG, Ramos-Godinez M del P et al. Internalization of titanium dioxide nanoparticles by glial cells is given at short times and is mainly mediated by actin reorganization-dependent endocytosis. *Neurotoxicology*. 2015;**51**:27–37. doi: 10.1016/j.neuro.2015.08.013.
57. Singh S, Shi T, Duffin R et al. Endocytosis, oxidative stress and IL-8 expression in human lung epithelial cells upon treatment with fine and ultrafine TiO_2: role of the specific surface area and of surface methylation of the particles. *Toxicol. Appl. Pharmacol*. 2007;**222**:141–51. doi: 10.1016/j.taap.2007.05.001.